

Abstract

This article reviews enhanced wireless access technologies and experimental evaluations of the wideband DS-CDMA physical layer employing intercell asynchronous operation with a three-step fast cell search method, pilot symbol-assisted coherent links, signal-to-interference plus background noise power ratio-based fast transmit power control, site diversity (soft/softer handover), and transmit diversity in the forward link. The article also presents link-capacity-enhancing techniques such as using an interference canceller and adaptive antenna array diversity receiver/transmitter, and experimental results in a real multipath fading channel. The laboratory and field experiments exemplify superior techniques of the W-CDMA physical layer and the potential of the IC and AAAD transceiver to decrease the mobile transmit power in the reverse link and multipath interference from high-rate users with large transmit power in the forward link.

Enhanced Wireless Access Technologies and Experiments for W-CDMA Communications

MAMORU SAWAHASHI, KENICHI HIGUCHI, AND SHINYA TANAKA,
NTT DoCoMo, Inc.

FUMIYUKI ADACHI, TOHOKU UNIVERSITY

The amazing increase in the number of "i-mode service" customers using the personal digital cellular (PDC) system in Japan indicates that major services provided by second-generation systems will migrate from voice services to multimedia data transmission over the Internet. As we enter the 21st century, the demand will continue to increase for a variety of wideband services (e.g., Internet access and the transmission of video and high-quality images from/to moving vehicles). International Mobile Telecommunications in 2000 (IMT-2000) is expected to meet these demands. Wideband code-division multiple access (W-CDMA) [1] is adopted as a wireless access technique for the frequency-division duplex (FDD) mode of IMT-2000 [2]. Direct sequence CDMA (DS-CDMA) wireless access, on which W-CDMA is based, has numerous advantages over time- or frequency-division multiple access (TDMA, FDMA), including single frequency reuse, soft handoff (or site diversity), enhanced radio transmission through Rake combining, and direct capacity increase by sectorized antennas. Standardization and development of the W-CDMA commercial system is continuing with enthusiastic efforts aimed at commercial service in the 3rd Generation Partnership Project (3GPP). Key features of the W-CDMA physical layer are:

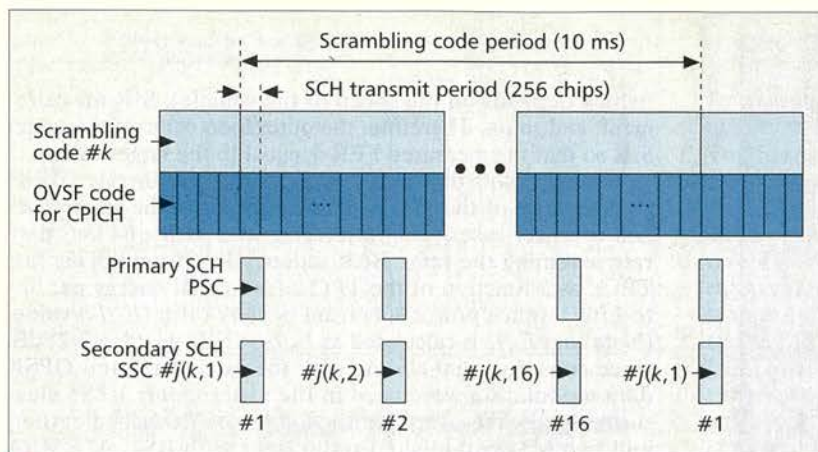
- Intercell asynchronous operation and three-step fast cell search
- Large gains in link capacity and coverage through the use of coherent detection (in the forward and reverse links) and signal-to-interference (plus background noise power) ratio (SIR)-based fast transmit power control (TPC)
- High flexibility in offering different multirate services (up to 2 Mb/s) through orthogonal variable spreading factor (OVSF) multiplexing and orthogonal multicode transmission
- Capacity-enhanced techniques such as interference cancellation (IC) and adaptive antenna array diversity (AAAD)

The above key W-CDMA technologies associated with its performance and the features of the W-CDMA air interface were comprehensively overviewed in [1]. However, in the ongoing standardization process worldwide in 3GPP, the radio link parameters and channel structure were modified, and enhanced techniques such as turbo coding applications for high-rate data transmission and transmit diversity were adopted into the standards. Therefore, this article overviews the enhanced wireless access technologies of W-CDMA, focusing on verification of the link performance of these technologies through a series of laboratory and field experiments conducted in an area near Tokyo based on an implemented W-CDMA experimental system using the 2 GHz carrier frequency band. We designed and developed an experimental system of a coherent multistage interference canceller (COM-SIC) and coherent adaptive antenna array diversity (CAAAD) receiver in the reverse link, and adaptive antenna array transmit diversity (AAA-TD) in the forward link in order to demonstrate the suppression effect on multiple access interference (MAI) and multipath interference (MPI). The experimental results of these techniques are also introduced.

Key Wireless Access Technologies in W-CDMA

Asynchronous Cell Sites and the Three-Step Cell Search Method

In asynchronous cell site operation, flexible system deployment from outdoors to indoors is possible, since no external timing source such as the global positioning system (GPS) is required. To allow asynchronous cell site operation, two-lay-



■ Figure 1. The forward link frame structure.

ered spreading code allocation is used [1]. In the forward link, cell sites are distinguished by their unique scrambling codes, and data channels (control and traffic channels) in each cell site are distinguished by different OVFS codes [9]. To reduce the cell search time in asynchronous cell site operation, we proposed a three-step cell search method using scrambling code masking [3]. Subsequently, our original cell search method was refined in the standardization process. The forward link frame structure in the 3GPP standard required for the three-step cell search is illustrated in Fig. 1. The base station (BS) transmits the continuous common pilot channel (CPICH), primary synchronization channel (SCH), and secondary SCH over the 256-chip duration at the beginning of each slot (every 0.625 ms). The spreading codes for the CPICH and dedicated physical channels (DPCHs) were taken from a set of OVFS codes, thereby maintaining mutual orthogonality between CPICH and DPCHs. These channels were further scrambled by a cell-specific scrambling code with a 10 ms repetition period ($= 40,960$ -chip duration), which is equal to the data frame length. The primary synchronization code (PSC) for the primary-SCH is common to all cell sites; the secondary synchronization code (SSC) for the secondary SCH denotes the group index into which each scrambling code is grouped beforehand. The total number of scrambling codes to be searched was 512, which was divided into 32 groups of 16 codes each. The transmit powers of the primary and secondary SCH were set to half that of the CPICH.

Using the SCHs and CPICH, the three-step cell search is performed as follows. First, the PSC matched filter (MF) is used. The MF output was averaged over period T_1 to detect the primary SCH time position that provides the maximum average correlation. Next, the scrambling code group was identified by taking the cross-correlation between the received signal and the set of SSCs over period T_2 . Finally, the scrambling code was identified by taking a partial correlation between the received signal and each of the candidate scrambling codes and then averaging over period T_3 . The scrambling code that provides the maximum correlation was determined as the scrambling code to be searched. To reduce false detection, a verification mode was added using a frame synchronization check. When the synchronization verification failed two consecutive times, the cell search process was restarted from the first step.

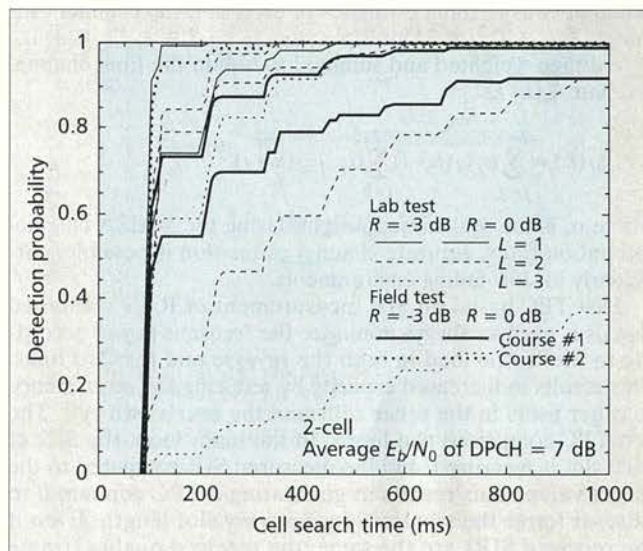
Figure 2 shows the measured field experimental results of the probability distribution of the cell search time with the transmit power ratio of CPICH to DPCH, R , as a parameter using the 4.096 Mc/s W-CDMA experimental system in asynchronous two-cell site environments with 20 simultaneous DPCHs transmitting without fast TPC. The antenna heights of

BS1 (BS2) and the mobile station (MS) are 59 (44) m and 2.9 m, respectively. The measurement courses were the same as in [1]. The test courses were approximately 700 (2.0) m to 1.1 (2.5) km away from BS1 (BS2). Test course #1 first exhibited clear two-path and single-path fading at the middle of the course for both BSs. Then three-path fading with unequal average power was observed at the end of the course. Along course #2, there was single-path fading for almost the entire duration from the start point to the middle and then followed by slight three-path fading at the end for BS1, while most of the course exhibited one- to two-path fading for BS2. A measurement vehicle equipped with the MS transceiver was driven at an average speed of

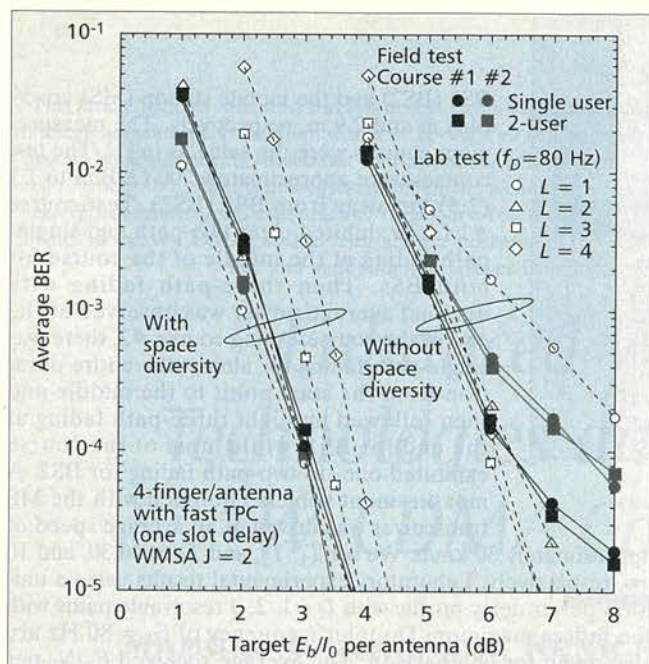
approximately 30 km/h. We set T_1 , T_2 , and T_3 to 40, 30, and 10 ms, respectively. Laboratory experimental results using a uniform power delay profile with $L = 1, 2, 3$ resolvable paths with the fading maximum Doppler frequency of $f_D = 80$ Hz are also given for comparison. The average received E_b/N_0 per DPCH of BS1 and BS2 over the measurement test courses were both 7 dB. Figure 2 shows that the field experimental results measured in course #1 (#2) were better than the laboratory experimental results when $L = 2$ (1), which is based on the observed power delay profile. This is explained below. In the two-cell case in the field experiments, although the average received E_b/N_0 values of SCH and CPICH over the course from two cell sites were equal, the instantaneous received signal powers of the two cell sites were different due to the independent shadowing variations. Therefore, the MS can search the scrambling code of the cell site with a larger received signal power utilizing the compensation effect of the received level degradation (i.e., site diversity effect). This effect is considered larger than the increase in interference from another cell. In the two-cell case, cell search can be completed within approximately 700 and 240 ms at 90 percent probability, when $R = -3$ dB, for course #1 and course #2, respectively.

Coherent Channel Estimation and SIR-Based Fast TPC

Pilot symbol assisted (PSA) coherent detection is used for both the reverse and forward links [1]. The received multipath



■ Figure 2. The probability distribution of the cell search time in field experiments.



■ **Figure 3.** Average BER as a function of target E_b/I_0 per antenna in field experiments.

signals are despread by the MF and resolved into L -multipath components of transmitted quadrature phase shift keyed (QPSK) modulated data that are received via different propagation paths with different delay times. The coherent Rake combiner output is expressed at the n th symbol position of the k th slot associated with the l th path ($l = 0, 1, \dots, L-1$) using despread signal $r_l(n, k)$ as

$$\tilde{d}(n, k) = \sum_{l=0}^{L-1} r_l(n, k) \tilde{\xi}_l^*(k), \quad (1)$$

where $\tilde{\xi}_l(k)$ represents the channel estimates. The output data sequence, $\tilde{d}(n, k)$, is deinterleaved and channel decoded to recover the transmitted binary data sequence. In order to achieve accurate channel estimation that works satisfactorily in a fast fading environment, we presented an improved channel estimation filter called a *weighted multislot averaging* (WMSA) channel estimation filter [4]. After obtaining the instantaneous channel estimates of each slot, the channel estimates, $\xi_l(j+i)$ s, of $2J$ multiple slots ($i = -J+1, \dots, 0, 1, \dots, J$), are then weighted and summed to obtain the final channel estimate $\tilde{\xi}_l(k)$ as

$$\tilde{\xi}_l(k) = \sum_{i=0}^{J-1} \alpha_i \xi_l(k-i) \sum_{i=0}^J \alpha_{i-1} \xi_l(k+i), \quad (2)$$

where α_i is the real-valued weight. Using the WMSA channel estimation filter, accurate channel estimation is possible, particularly in slow fading environments.

Fast TPC based on SIR measurement of Rake combined signals is used to always minimize the transmit power according to the traffic load in both the reverse and forward links. This results in increased capacity by reducing the interference to other users in the other cells and the user's own cell. The fast TPC comprised two loops. In the inner loop, the SIR of each slot is measured, and the measured SIR compared to the target value. This results in generating a TPC command to raise or lower the transmit power every slot length. Even if the received SIRs are the same, the received quality (frame error rate, FER) is not the same because the FERs are affected by the number of paths, maximum Doppler frequency

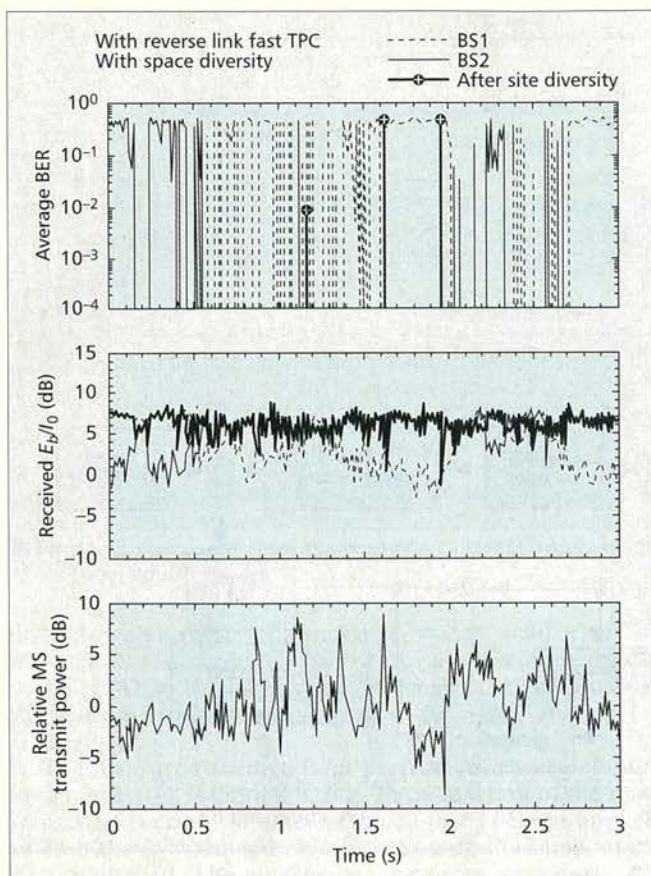
(which depends on the speed of the vehicle), SIR measurement, and so on. Therefore, the outer loop controls the target SIR so that the measured FER is equal to the target value.

Figure 3 plots the measured average bit error rate (BER) performance of the 32 kb/s data rate user in the single-user and two-user cases (one interfering user with a 64 kb/s data rate assuming the same BER independently employing fast TPC), as a function of the TPC target signal energy per bit-to-interference power spectrum density ratio (E_b/I_0) value. (Note that E_b/I_0 is calculated as $E_b/I_0 = \text{SIR} + 10\log(3/2)$ dB, since convolutional coding with the rate of 1/3 and QPSK data modulation were used in the experiments.) The measurement courses were identical to those described earlier, and two MSs established radio links with BS1. A WMSA channel estimation filter with $J = 2$ was used. Laboratory experimental results of the single-user case using the L -path model with $f_D = 80$ Hz are also plotted for comparison. The results clearly show that the target E_b/I_0 when the interfering user exists becomes almost the same to achieve the same BER as that of the single-user case, implying that the fast TPC worked satisfactorily in a real fading channel. The measured numbers of active Rake fingers per antenna along test courses #1 and #2 are 2.0 and 1.6, respectively. Figure 3 shows that the measured BER performance of course #1 is almost the same as the laboratory-measured BER performance when $L = 2$, and the measured BER performance of course #2 is found between the laboratory-measured BER performances when $L = 1$ and 2. The field-measured BER performances are in good agreement with those estimated from the laboratory experiment. The figure also shows that two-branch space diversity (antenna diversity) reception can reduce the target E_b/I_0 by approximately 3 dB at the average BER of 10^{-3} . With space diversity reception, the average BER of 10^{-3} can be achieved at the required E_b/I_0 of approximately 3 dB/antenna.

Site Diversity (Soft/Softer Handover)

Soft handoff or site diversity (site diversity hereafter), which was first implemented in the IS-95 CDMA standard [5], is an essential technique together with fast TPC in improving transmission impairment due to multipath fading and shadowing near the cell edge. In the forward link, the same original information data sequences before channel coding are transferred to N BSs (N is the number of BSs with which the MS is associated) through the backhaul (wired transmission line between the BS and radio network controller, RNC) from an RNC and transmitted from N BSs using different scrambling codes. The received signals after Rake combining at the MS are combined symbol by symbol with maximal ratio combining (MRC) followed by channel decoding. With intersector diversity in the reverse link, the Rake-combined signal of each sector is combined with MRC in the same way as in the forward link. On the other hand, in the reverse link intercell site diversity, a hard-decision data sequence after channel decoding at each BS is transferred to the RNC via the backhaul with the reliability information associated with each traffic channel. The transferred data sequences are selection-combined every selection period, according to the reliability information.

The performance of reverse link intercell site diversity depends on the type of reliability information used. Therefore, we presented a two-step selection combining (SC) scheme using two types of reliability information: cyclic redundancy check (CRC) results calculated over selection interval T_{SEL} and the average received SIR measured over interleaving interval T_{ILV} . In our scheme, we use the number of slots with a measured SIR value larger than the target value of fast TPC, N_{SIR} , that is, the number of TPC command bits to lower



■ **Figure 4.** Instantaneous time variations in the reverse link intercell site diversity in field experiments.

the transmit power, during T_{ILV} instead of the actual measured SIR value. This is because the transfer capacity in the backhaul required for the reliability information of intercell site diversity can be significantly decreased. The SC at the RNC was performed in two steps:

- Step 1: When multiple decoded data sequences transferred from N cell sites (BSs) indicate no CRC error, the one data sequence over T_{SEL} among the data sequences yielding the successful CRC result is selected.
- Step 2: When all the CRC results transferred from N BSs indicate frame error, the data sequence during T_{SEL} with the larger N_{SIR} over T_{ILV} is selected.

We evaluated the average BER performance of the 32 kb/s data rate channel in intercell site diversity by field experiments. The measurement course is a road running north and south, which passes through the middle of two BSs. The middle point of the measurement course is approximately 1300 and 1200 m apart from BS1 and BS2, respectively. On either side of the measurement course is a low-rise factory area. The view from BS1 was line-of-sight (LOS) except at the end of the course, while it was non-LOS (NLOS) from BS2 due to the tall buildings. We set the soft handover threshold to 3 dB. The difference in the measured average received signal powers from the two BSs was approximately 1 dB. Thus, the measurement course is a soft handover area within the prescribed threshold. The power delay profile with 1 (2) and 2 (1) paths were observed in the first and latter halves of the course from BS1 (BS2). We set $T_{SEL} = 10$ ms. In the experiments, fast TPC was used only in the reverse link.

The measured time variations of the instantaneous BER and received E_b/I_0 at BS1 and BS2, after intercell site diversity in the reverse link, and mobile transmit powers averaged over the frame length are plotted in Fig. 4. The target E_b/I_0 after

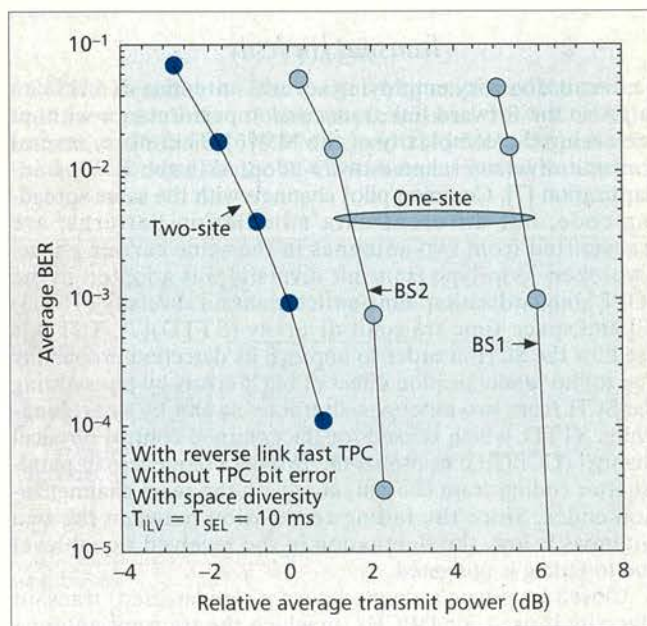
Rake combining at each BS was set to 7 dB so that the average BER after intercell site diversity was approximately 10^{-3} . The figures show that bit errors occurred when the received E_b/I_0 at each BS dropped. However, the instantaneous received E_b/I_0 after intercell site diversity was maintained at an almost constant level. Thus, the measured BER after intercell site diversity significantly improved over that of each BS. The measured average BER performance during intercell site diversity is shown in Fig. 5 as a function of the relative transmit power of the MS, which was normalized by that when the average BER of 10^{-3} was achieved during intercell site diversity. The performance when only a one-site connection with BS1 or BS2 was established is also plotted. These measured values were obtained by changing the target E_b/I_0 value. Although the received signal powers from BS1 and BS2 are almost equal, the BER performance when the radio link is connected to BS2 is better than with BS1 since the received signal power from BS2 is greater than that from BS1 in the longer part of the measurement course. Figure 5 shows that the required transmit power of the MS satisfying the average BER of 10^{-3} in intercell site diversity can be decreased by approximately 2.0 dB compared to that in the one-site connection.

When fast TPC is applied in the forward link intercell site diversity mode, each BS independently follows the TPC command bit sent from the MS via the reverse link. Therefore, the transmit power of each BS differs when a TPC command bit error occurs in the reverse link. An increase in the difference between the transmit powers of the BSs causes a reduction in site diversity gain and an increase in interference to other users. To overcome this problem, we proposed the following two-loop algorithm, shown in Fig. 6, to reduce the impact of TPC errors and keep the transmit power of the BSs the same.

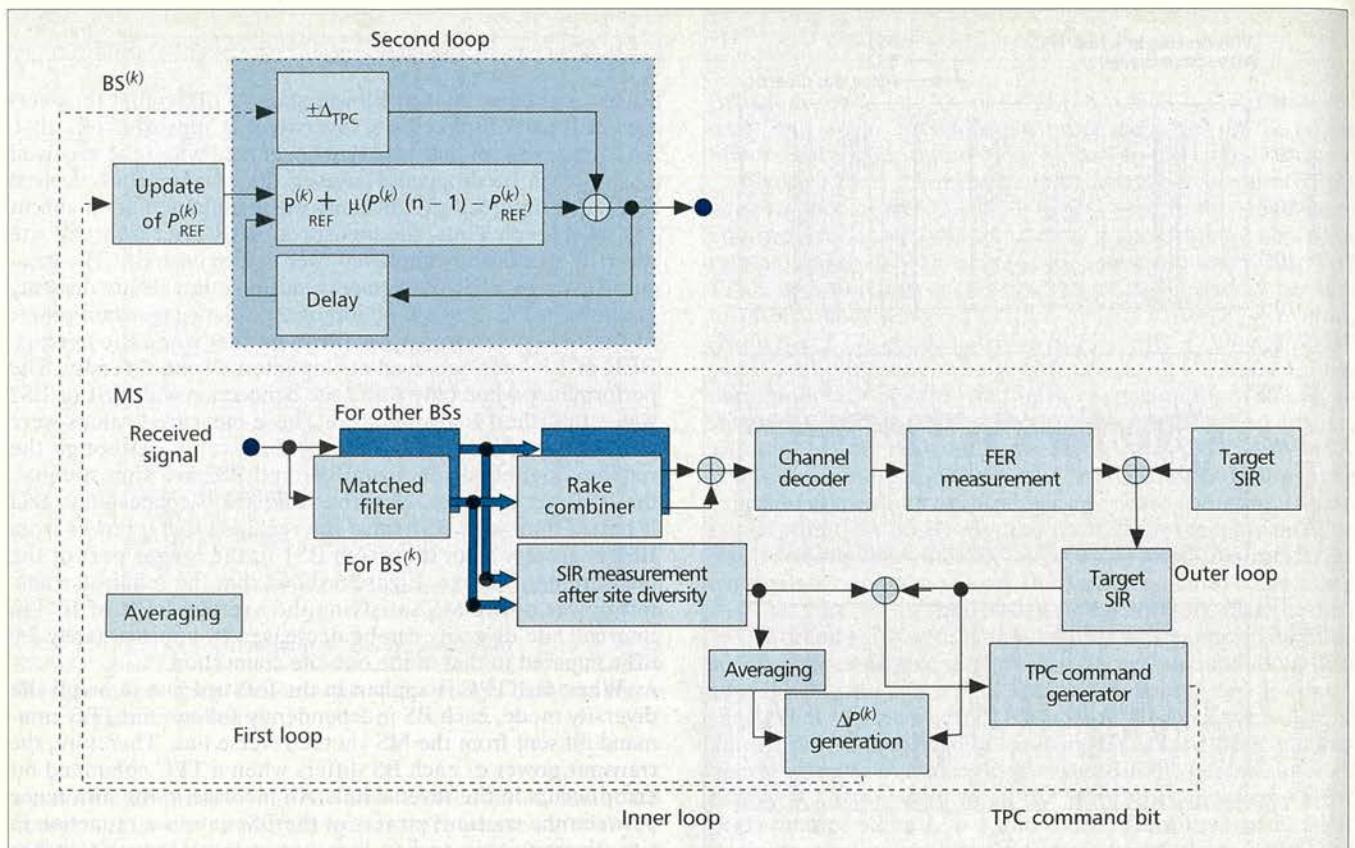
- First loop: The standard transmit powers, $P^{(k)}_{REF}$, of all BS_k are compensated by $\Delta P^{(k)}$ (dB) according to the dedicated control channel from a mobile based on the average SIR measurement at an MS,

$$\Delta P^{(k)} = \text{Target}_{E_b/I_0} - \text{Measured_total}_{E_b/I_0} \text{ (dB)}, \quad (3)$$

where the $\text{Measured_total}_{E_b/I_0}$ and Target_{E_b/I_0} are the measured E_b/I_0 after Rake combining and target E_b/I_0 at an



■ **Figure 5.** Average BER in the reverse link intercell site diversity in field experiments.



■ Figure 6. Combination of forward link site diversity and TPC.

MS, respectively. The $P_{\text{REF}}^{(k)}$ is constant during G -slot length and its value of n ($= g \times G$)th slot $P_{\text{REF}}^{(k)}(n)$ is updated every G -slot as $P_{\text{REF}}^{(k)}(g \times G) = P_{\text{REF}}^{(k)}((g-1) \times G) + \Delta P^{(k)}$.

- Second loop: The instantaneous transmit power, $P_{\text{CL}}^{(k)}(n)$, is controlled according to the TPC command bits (ΔP_{TPC}) by introducing forgetting factor μ using the standard transmit power compensated in the first loop,

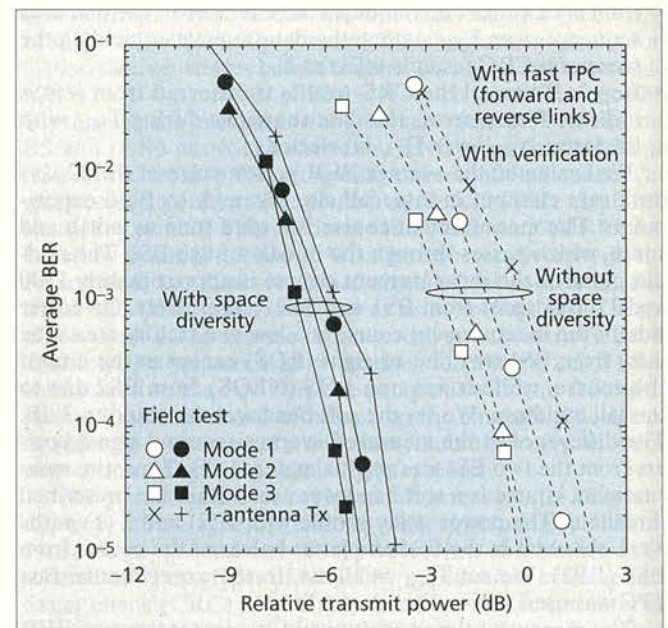
$$P_{\text{CL}}^{(k)}(n) = P_{\text{REF}}^{(k)} + \mu (P_{\text{CL}}^{(k)}(n-1) - P_{\text{REF}}^{(k)}) + \Delta P_{\text{TPC}}. \quad (4)$$

Transmit Diversity

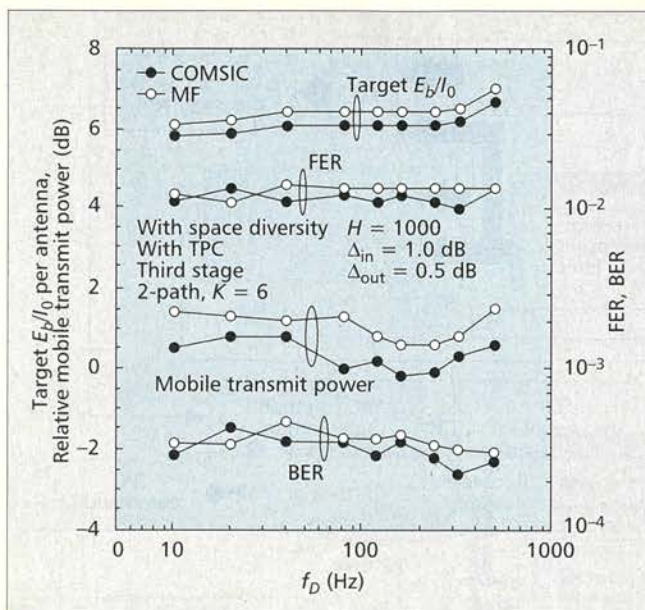
Transmit diversity employing several antennas at a BS can improve the forward link transmission performance without increasing the complexity of the MS [6]. Therefore, several transmit diversity schemes were adopted in the 3GPP standardization [7]. Common pilot channels with the same spreading code, but different data modulation patterns, are transmitted from two antennas in the same carrier phase. Two-open-loop-type transmit diversity was adopted in the 3GPP standardization: time-switch transmit diversity (TSTD) [7] and space-time transmit diversity (STTD)[7]. TSTD is used for the SCH in order to improve its detection probability due to the randomization effect of burst errors by transmitting the SCH from two antennas alternatively slot by slot. Meanwhile, STTD, which is used for the common control physical channel (CCPCH), transmits the two data sequences in parallel after coding from two antennas with the same channelization codes. Since the fading correlation between the two antennas is low, the fluctuation in the received signal level due to fading is mitigated.

Closed-loop-type (two modes were standardized) transmit diversity is used for DPCHs, in which the transmit antenna weights are controlled by the feedback information (FBI) generated at the MS [7]. In this article, three modes are consid-

ered for generating the transmit antenna weights. Let $W_1 = A_1 e^{j\phi_1}$ and $W_2 = A_2 e^{j\phi_2}$ be the transmit antenna weights. Thus, in mode 1, the transmitted phase of the second antenna, ϕ_2 , is changed with the accuracy of $\pi/4$ according to the FBI from the MS so that the received SIR after combining is maximum. This is expressed as $\phi_1 = 0$, $\phi_2 = \{\pm\pi/4, \pm3\pi/4\}$, $A_1 = A_2 = \sqrt{1/2}$. Mode 2 also incorporates adaptive transmitting phase



■ Figure 7. Average BER performance as a function of total BS transmit power in closed-loop-type transmit diversity in field experiments.



■ **Figure 10.** Average BER performance with fast TPC using the outer loop.

Since the detailed parameters and frame structure are given in [13], the following focuses only on the COMSIC receiver. The overall block diagram of the experimental COMSIC receiver with SF = 16 is illustrated in Fig. 8. At the receiver, the composite spread signal comprising all user spread signals was received by two antennas, each filtered by a square-root raised cosine Nyquist filter, and sampled at the rate of 4×1.024 MHz. The output signal of the COMSIC block is deinterleaved and then soft-decision Viterbi decoded to recover the transmitted data sequence. Fast TPC based on SIR measurement was used to decrease the transmit power of the MS. The implemented three-stage COMSIC receiver has a long processing delay (note that even for the parallel type, a processing delay much longer than the slot interval is necessary), although only a short TPC delay is required to decrease the TPC error. Therefore, in our scheme, the SIR measurement for fast TPC is performed at the MF output to achieve a one-slot delay to the conventional MF receiver. Since the SIR at the canceller output is much larger than that at the MF output, the target SIR is compensated by the outer loop so that the measured FER at the canceller output becomes the required value.

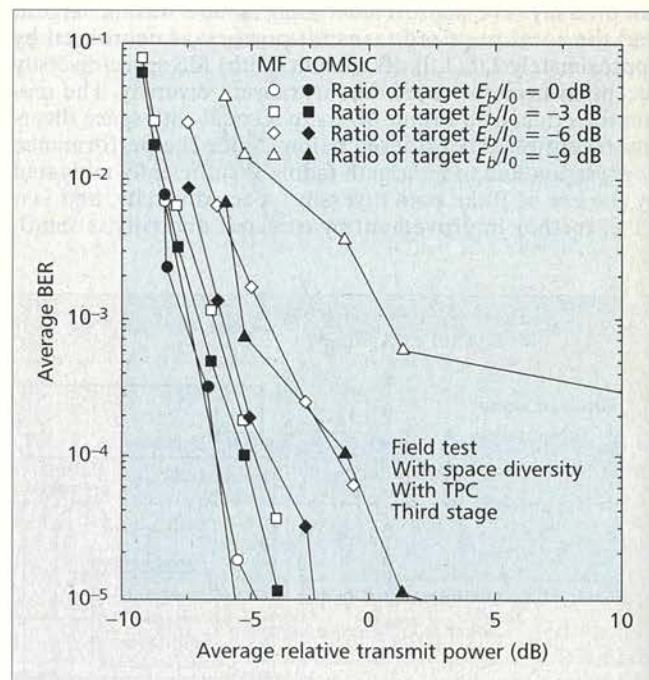
The COMSIC block comprises a channel ranking block and SF-parallel channel estimation and interference replica generation units (CEIGUs), one for each user at each stage. A sample sequence of the composite spread signal received at each antenna was despread using MFs to measure the received signal power of each user using both pilot and information data symbols in each slot in order to rank the users according to the received signal powers. Before CEIGU processing of each user, the generated replicas of other user interference were removed from the received composite spread signal. A detailed block diagram of the CEIGU is illustrated in Fig. 9. In each CEIGU, after removing the estimated MAI replica $I_u^{(x)}(p)$ at the previous (same) stage for higher (lower) ranking, user # u (p and x ($= 0, 1$) denote the stage number and space diversity branch, respectively), the input signal was despread by MFs into independent resolved path components for each space diversity branch. The Rake fingers were assigned to two paths per antenna at maximum, which provides an average signal power larger than three times the background noise plus interference power (this threshold value was optimized in

the experiments). The channel variation of each path was estimated using a PSA channel estimation filter and then coherently Rake-combined. A tentative data decision was performed for the Rake-combined signal, and the interference replica of each path was regenerated using this tentative decided data modulation, channel estimates, and the estimated received timing of each path.

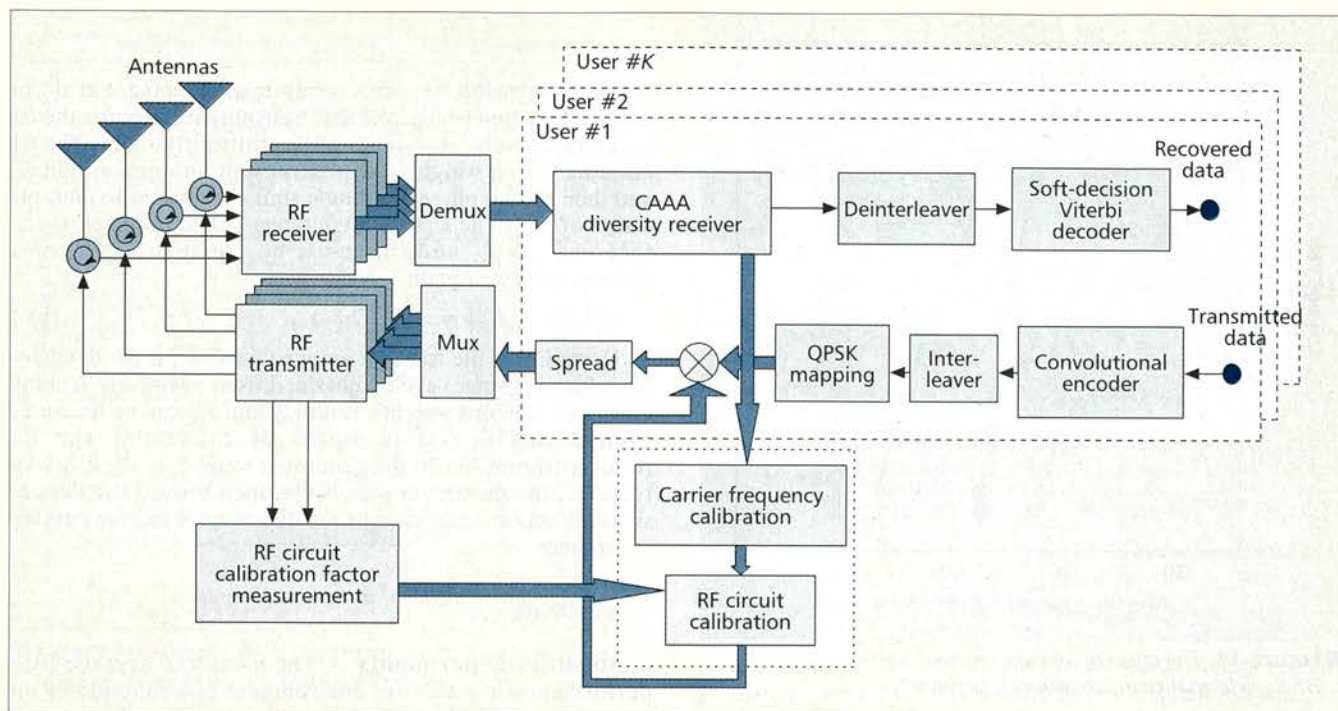
Experimental Results

Laboratory Experiments — The average BER performance of the COMSIC receiver using two-branch space diversity reception was evaluated through laboratory experiments using a fading simulator. External Gaussian noise was added as background noise to the receiver input. The power delay profile used here was a two-path profile, each path being subjected to independent Rayleigh fading with equal average power. The receiver performance using fast TPC with space diversity reception was investigated for the number of active users, $K = 6$. The measured FER, BER, target E_b/I_0 , and MS transmit power are shown in Fig. 10 as a function of f_D . The required FER was set to 10^{-2} . The step size of the inner and outer loops were set to $\Delta_{in} = 1.0$ dB and $\Delta_{out} = 0.5$ dB, respectively. The TPC delay was assumed to be two slots. The threshold and averaging time for the FER calculation in a frame were $M = 8/1000$ and $H = 1000$, respectively. Figure 10 shows that average FER and BER performance were accurately controlled to be the required value over a wide range of f_D (10–500 Hz), while the target E_b/I_0 varies with the range of approximately 2 dB. The transmit power of the MS for the COMSIC receiver is decreased by about 0.8 dB from that of the MF-based Rake receiver, since it reduces the MAI.

Field Experiments — Field experiments on the COMSIC receivers in the reverse link were conducted near Tokyo using two MSs (one interfering MS). The measurement course of the desired MS was course #1, described earlier, while the



■ **Figure 11.** Average BER performance as a function of relative MS transmit power in field experiments.

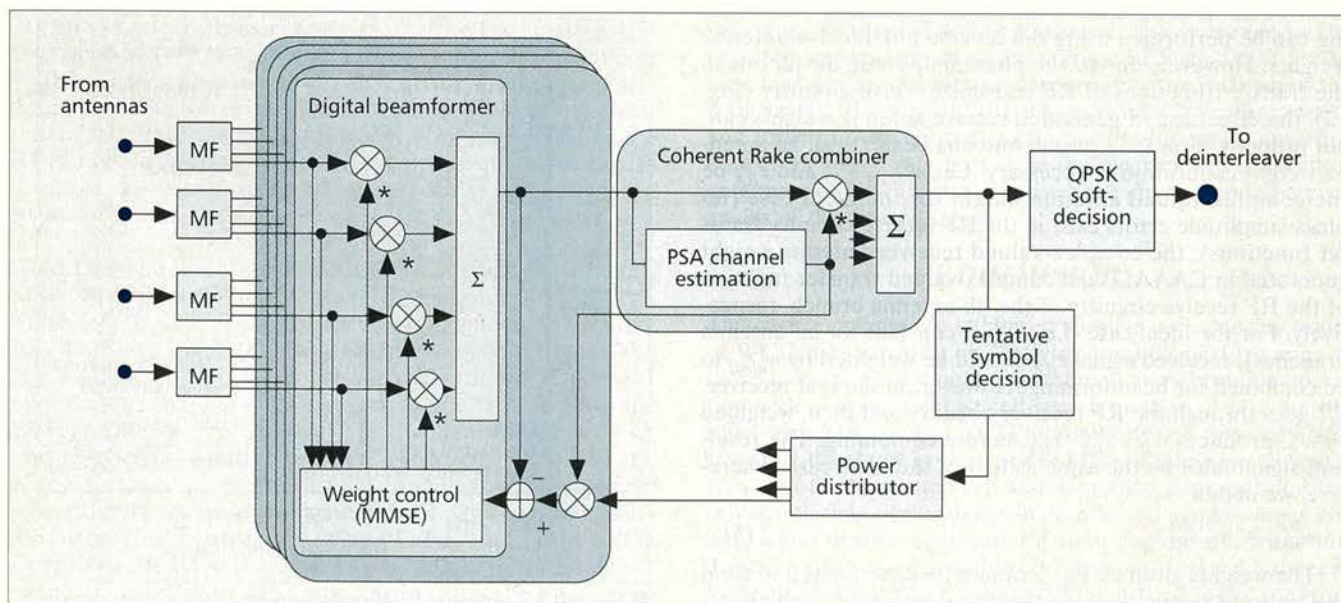


■ **Figure 12.** An overall block diagram of a CAAAD transceiver.

interfering MS was located at a fixed point approximately 100 m from the BS. A measurement vehicle equipped with the desired MS transceiver was driven at an average speed of approximately 30 km/h. Figure 11 plots the measured average BER performance as a function of the relative transmit power of an MS with fast TPC and space diversity reception. The figure shows that the MS transmit power of the MF-based Rake receiver increased due to the increased MAI as the ratio of target E_b/I_0 s decreased, while the COMSIC receiver decreased the required MS transmit power for the average BER of 10^{-3} by approximately 2.0 (4.0) dB compared to the MF receiver when the ratio of target E_b/I_0 s = -6 (-9) dB. This implies that the COMSIC receiver is effective in decreasing the MS transmit power when an interfering user with a large transmit power exists.

AAAD

CAAAD Receiver/AAA-TD — We also investigated the interference suppression effect in the reverse and forward links using the experimental CAAAD receiver/AAA-TD [14, 15]. The carrier frequencies are the same as those of the COMSIC. The spreading chip rate was 4.096 Mc/s, and the bandwidth was 5 MHz. Figure 12 shows an overall block diagram of the four-antenna CAAAD transceiver. In the receiver, the baseband in-phase (I) and quadrature-phase (Q) components were sampled at the rate of 4×4.096 MHz. Figure 13 shows a block diagram of the digital beam former and Rake combiner in the CAAAD receiver. This block comprises MFs, a beamformer, PSA-coherent Rake combiner, and weight controller. The MF output signal samples of all



■ **Figure 13.** A block diagram of CAAAD processing.

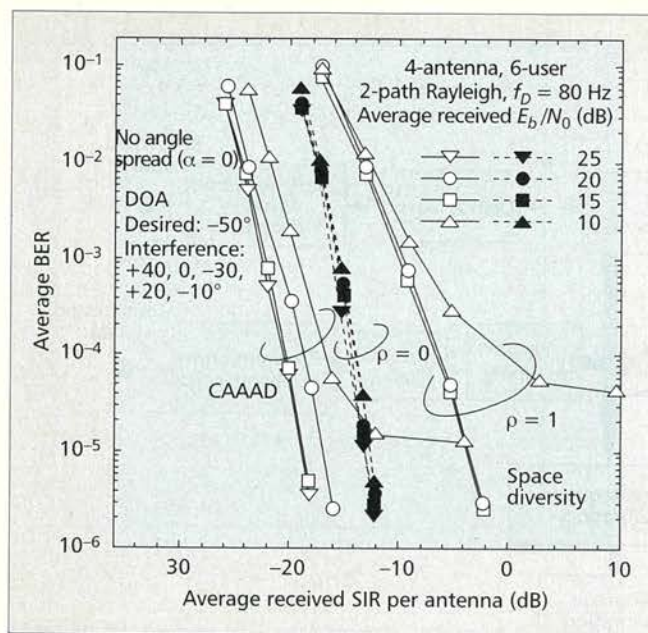


Figure 14. The effect of average received E_b/N_0 on average BER performance in laboratory experiments.

antennas for each resolved path are weighted and combined by the beamformer to form a received antenna beam pattern so that the average SIR of the combined signal associated with each resolved path is maximized. The resulting composite channel gain at the beamformer output is estimated by using pilot symbols of two successive slots for coherent Rake combining of different resolved paths. The antenna weights in the CAAAD receiver are updated every four symbols using the Normalized Least Mean Square (N-LMS) algorithm. The weight adaptation algorithm is described in [14]. Periodically received pilot symbols and tentatively decided data symbols after Rake combining are used to generate the reference signal.

In the transmitter, the coded data are weight-multiplied in the baseband processing block. After conversion into an analog signal, this baseband analog signal is modulated by a quadrature modulator and amplified by the power amplifier. Since the instantaneous channel variation due to fading is not involved in the reverse link beamforming, transmit beamforming can be performed using the reverse link receive antenna weights. However, due to the phase/amplitude deviations in the transfer functions of RF transmit/receive circuitry (Fig. 12), the direct use of generated receive antenna weights cannot properly form the transmit antenna beam; thus, an antenna weight calibration is necessary. Let $w_{ideal}^{(i)}$, $w_R^{(i)}$, and $x_{RX}^{(i)}$ be the complex-valued antenna weight for the ideal case (no phase/amplitude errors exist in the RF receive circuitry transfer functions), the complex-valued receiver antenna weight generated in CAAAD, and complex-valued transfer function of the RF receive circuitry of the i th antenna branch, respectively. For the ideal case (i.e., $x_{RX}^{(i)}$ = constant for all antenna branches), received signal $r_{RX}^{(i)}$ should be weighted by $w_{ideal}^{(i)}$ to be combined for beamforming. However, in the real receiver, $r_{RX}^{(i)}$ goes through the RF receiver circuitry and then, weighted by $w_R^{(i)}$, produces $w_R^{(i)} \cdot x_{RX}^{(i)} \cdot r_{RX}^{(i)}$, before combining. The resultant signal must be the same as that of the ideal case. Therefore, we obtain

$$w_{ideal}^{(i)} = w_R^{(i)} x_{RX}^{(i)} \quad (5)$$

The weights given by Eq. 5 cannot be directly used to form the transmit beam, because the signal weighted at the baseband stage suffers phase/amplitude shift due to the RF trans-

mit circuitry before transmission from an antenna. Let $x_{TX}^{(i)}$ be the transfer function of the RF transmit circuitry for the i th antenna branch. The signal to be transmitted from the i th antenna is first weighted using transmit antenna weight $w_T^{(i)}$ and then suffers phase/amplitude shift (equivalent to multiplication of $x_{TX}^{(i)}$). The equivalent antenna weight becomes, therefore, $w_T^{(i)} \cdot x_{TX}^{(i)}$, and this must be equal to $w_{ideal}^{(i)}$. As a consequence, we obtain

$$w_T^{(i)} = w_{ideal}^{(i)} / x_{TX}^{(i)} = w_R^{(i)} (x_{RX}^{(i)} / x_{TX}^{(i)}) \quad (6)$$

Using Eq. 6, the transmit antenna weights (at the baseband beamforming stage) can be obtained from adaptively generated receive antenna weights. Both $x_{RX}^{(i)}$ and $x_{TX}^{(i)}$ can be measured even during operation mode. By calibrating the RF receiver/transmitter to the generated weights in the CAAAD receiver, the maximum gain is obtained toward the desired signal direction, and the nulls are directed toward the interfering sources.

Experiments

Laboratory Experiments — The measured average BER performance in a six-user environment as a function of the average received SIR at each antenna with an angle spread of 0° is shown in Fig. 14 with the average received E_b/N_0 of the desired user (MS1) as a parameter. The directions of arrival (DOAs) of MSs 1, 2, 3, 4, 5, and 6 were set to -50° , -30° , -10° , 0° , $+20^\circ$, and $+40^\circ$, respectively. A two-path profile with equal average power was assumed, with each path subjected to independent Rayleigh fading with $f_D = 80$ Hz. The BER performance of a four-branch space diversity receiver using MRC with fading correlation, $\rho = 0$, is also plotted for comparison. Even when the number of interfering users is larger than that of the beam nulls, it is clear that the required average received SIR of the CAAAD receiver for achieving the average BER of 10^{-3} can be reduced by approximately 6 dB compared to space diversity reception with MRC when the average received $E_b/N_0 = 20$ dB. The BER performance of the CAAAD receiver is inferior to that of space diversity with $\rho = 0$ in the noise limited region due to the lack of

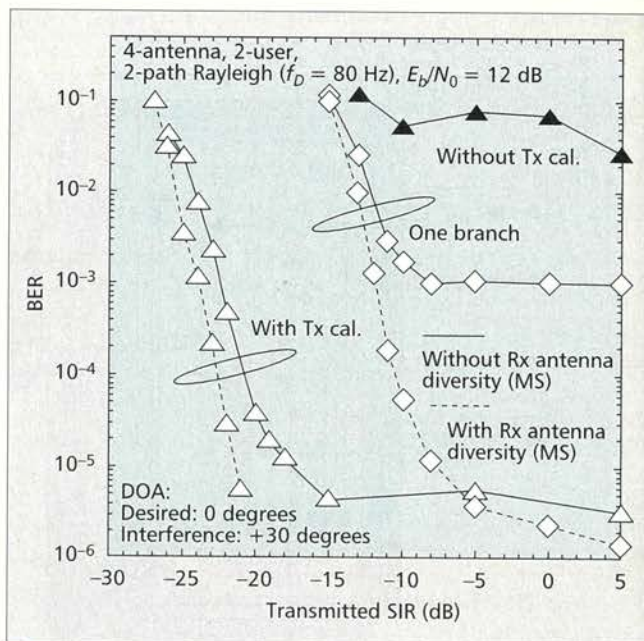
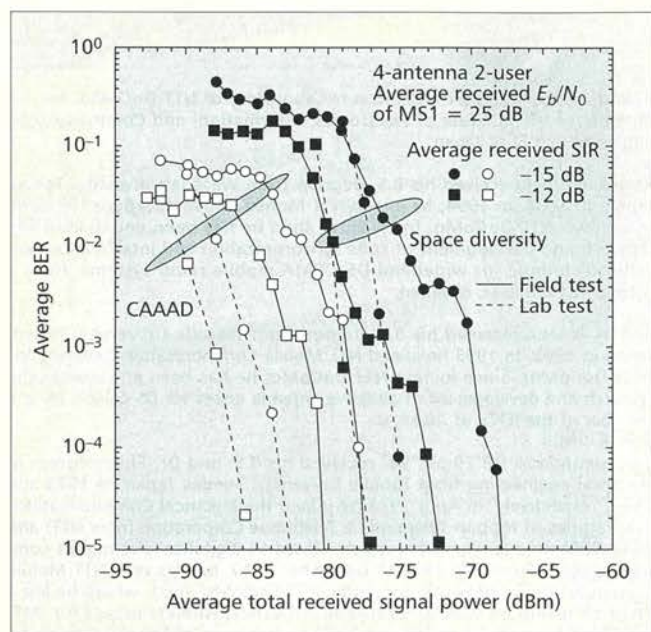


Figure 15. Average BER performance as a function of transmitted SIR before weighting in laboratory experiments.

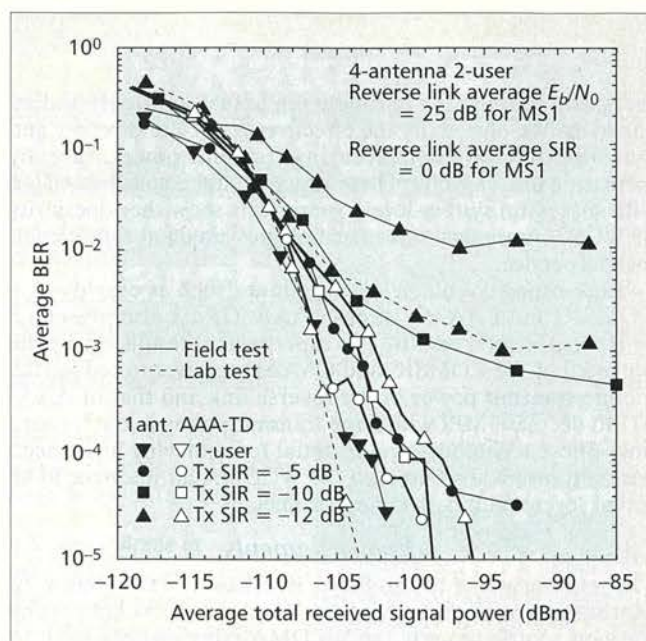


■ **Figure 16.** Average BER performance as a function of average received signal power in field experiments.

diversity effect since fading correlation among the antenna elements is almost one. However, we experimentally demonstrated when fast TPC is used, CAAAD is superior to space diversity for a wide range of E_b/N_0 under low-to-high SIR conditions [16].

Next, we evaluated the forward link performance using AAA-TD. The experimental configuration of AAA-TD is described in [15]. The DOAs of MS1 (desired user) and MS2 (interfering user) are set to 0° and $+30^\circ$, respectively. A two-path profile with equal average power was assumed, each path being subjected to independent Rayleigh fading with $f_D = 80$ Hz. Figure 15 shows the measured average BER performance for MS1 as a function of the transmitted SIR before weighting. The BER performance without calibrating the RF transmitter circuitry and that transmitted by an omnidirectional antenna are also shown for comparison. Two-branch space diversity reception and a two-finger Rake receiver were assumed for the MSs, and forward link TPC was not employed. From the figure, when the transmitted SIR = -10 dB, the required transmitted SIR for the average BER of 10^{-3} when AAA-TD is applied is improved by approximately 12 dB. This is because the transmitting gain toward the desired user improves and the interfering signal in the direction of the other users is suppressed. Without calibrating the RF transmitter circuitry, the BER performance degrades because the transmitted beam pattern is not generated toward the desired user.

Field Experiments — In the CAAAD receiver experiments, MS1 (desired user) moved along the measurement course, which was located approximately 600–850 m away from the BS. The height of the BS antenna was 50 m from the ground, and 120° sectored antennas were used. When MS1 moved along the measurement course, the DOA toward the BS changed from -10° to $+10^\circ$. In the measurement course, one-to-two path fading appeared in the first half of the course followed by two-to-three path fading with an average power difference of approximately 3 dB. On the other hand, MS2 (interfering user) was located at a fixed point 600 m away from the BS and almost in the LOS path (thus, single-path). The DOA of MS2 was approximately $+40^\circ$. The measured BER performance is plotted in Fig. 16 as a func-



■ **Figure 17.** BER performance as a function of average received signal power in field experiments; reverse link SIR = 0 dB.

tion of the average received signal power with the average received SIR of MS1 as a parameter. For comparison, the results of space diversity using MRC are also plotted (antenna separation was 10λ ; λ was a carrier wavelength in the reverse link). It can be understood from Fig. 16 that the required average received signal power for obtaining the average BER of 10^{-3} can be decreased by approximately 8–10 dB using the CAAAD receiver compared to using space diversity.

The average BER performance measured at an MS using AAA-TD in the forward link is plotted in Fig. 17 as a function of the average received signal power when the average received SIR of MS1 was 0 dB. The transmitted SIR of MS1 before weighting was -5 , -10 , and -12 dB. The BER performance of a one-antenna transmitter is also shown in the figure. The figure clearly shows that although the BER performance with the 1-antenna transmitter was severely degraded as the transmitted SIR was decreased, it was significantly improved by using AAA-TD due to beam and null steering. When AAA-TD was used, the increase in the required transmit power at the average BER of 10^{-3} from the case without an interfering user was within 5 dB when the transmitted SIR was -12 dB. These results from the reverse and forward links verify the effects of reducing the interference from a high-rate user since the receiver and transmitter antenna weights can precisely track the changes in the arrival angles of the desired signal.

Conclusion

This article reviews the enhanced wireless access technologies of WCDMA, focusing on verifying the link performance of these technologies, employing intercell asynchronous operation with a three-step fast cell-search method, PSA coherent links with SIR-based fast TPC, intercell site diversity, and transmit diversity in the forward link. Field experimental results of the three-step cell search method demonstrated fast cell search time performance in an intercell asynchronous system, while flexible continuous system deployment from outdoors to indoors is possible. Pilot-symbol-based coherent Rake reception proved to give efficient (i.e., lower required E_b/I_0) transmission together with fast TPC and space diversity

reception based on experiments in actual multipath fading channels. We also verify the effectiveness of site diversity and transmit diversity in decreasing transmit power, thereby increasing link capacity. These experimental results associated with successful system-level experiments show the superiority of WCDMA physical layer technologies aimed at future commercial service.

Link-capacity-enhancing techniques such as employing a COMSIC and CAAAD receiver/AAA-TD are also presented with experimental results. The experimental results clarify the potential of the COMSIC and CAAAD receiver to reduce the mobile transmit power in the reverse link and that of AAA-TD to decrease MPI with large transmit power in the forward link. These techniques are essential for achieving high-speed packet transmission based on the WCDMA air interface in an actual severe multipath fading channel.

Acknowledgments

The authors would like to thank K. Okawa, S. Fukumoto, A. Morimoto, and A. Harada of the Wireless Access Laboratory for their contributions to the WCDMA experiments.

References

- [1] F. Adachi, M. Sawahashi, and H. Suda, "Wideband DS-SS-CDMA for Next Generation Mobile Communication System," *IEEE Commun. Mag.*, vol. 36, Sept. 1998, pp. 56-69.
- [2] Special Issue, "Standards efforts of the ITU," *IEEE Pers. Commun.*, vol. 4, Aug. 1997.
- [3] K. Higuchi, M. Sawahashi, and F. Adachi, "Fast Cell Search Algorithm in DS-SS-CDMA Mobile Radio Using Long Spreading Codes," *IEICE Trans. Commun.*, vol. E81-B, July 1998, pp. 1527-34.
- [4] H. Andoh, M. Sawahashi, and F. Adachi, "Channel Estimation Filter Using Time-Multiplexed Pilot Channel for Coherent Rake Combining in DS-SS-CDMA Mobile Radio," *IEICE Trans. Commun.*, vol. E81-B no. 7, July 1998, pp. 1517-26.
- [5] TTA/EIA/IS-95, "Mobile Station-Base Station Compatibility Standard for Dual-Mode Wideband Spread Spectrum Cellular System," July 1993.
- [6] S. Fukumoto et al., "Field Experiments on Closed Loop Mode Transmit Diversity in W-CDMA Forward Link," submitted to *IEEE ISSSTA'2000*.
- [7] 3GPP RAN, 3G TS 25.211 V3.2.0, Mar. 2000.
- [8] ETSI SMG2 UMTS-L1, "Downlink Transmit Diversity," Tdoc 128/98, May 1998.
- [9] K. Okawa and F. Adachi, "Orthogonal Forward Link Using Orthogonal Multi-Spreading Factor Codes for Coherent DS-SS-CDMA Mobile Radio," *IEICE Trans. Commun.*, vol. E81-B, Apr. 1998, pp. 777-84.
- [10] A. Duel-Hallen, J. Holtzman, and Z. Zvonar, "Multiuser Detection for CDMA Systems," *IEEE Pers. Commun.*, Apr. 1995, pp. 46-58.
- [11] M. Sawahashi et al., "Pilot Symbol-Assisted Coherent Multistage Interference Canceller Using Recursive Channel Estimation for DS-SS-CDMA Mobile Radio," *IEICE Trans. Commun.*, vol. E79-B, Sept. 1996, pp. 1262-70.
- [12] G. V. Tsoulos, M. A. Beach, and J. McGeehan, "Wireless Personal Communications for the 21st Century: European Technological Advances in Adaptive Antennas," *IEEE Commun. Mag.*, Sept. 1997, pp. 102-9.
- [13] M. Sawahashi et al., "Experiments on Coherent Multistage Interference Canceller for DS-SS-CDMA Mobile Radio," *IEEE PIMRC '98*, Boston, MA, Sept. 8-11, 1998, pp. 491-96.
- [14] S. Tanaka, M. Sawahashi, and F. Adachi, "Pilot Symbol-assisted Decision-directed Coherent Adaptive Array Diversity for DS-SS-CDMA Mobile Radio Reverse Link," *IEICE Trans. Fundamentals*, vol. E80-A, Dec. 1997, pp. 2445-54.
- [15] A. Harada et al., "Performance of Adaptive Antenna Array Diversity Transmitter for W-CDMA Forward Link," *IEEE PIMRC '99*, Osaka, Japan, Sept. 12-15, 1999, pp. 1134-38.
- [16] S. Tanaka et al., "Combined Effect of Coherent Adaptive Antenna Array Diversity Receiver and Fast Transmit Power Control in W-CDMA Reverse Link," *Proc. VTC 2000*, Tokyo, Japan, May 2000, pp. 2147-51.

Biographies

MAMORU SAWAHASHI (sawahashi@mlab.yrp.nttdocomo.co.jp) (M'88) received his B.S. and M.S. degrees from Tokyo University in 1983 and 1985, respectively, and his Dr. Eng. degree from the Nara Institute of Technology in 1998. In 1985 he joined NTT Electrical Communications Laboratories, and in 1992 he transferred to NTT Mobile Communications Network, Inc. (now, NTT DoCoMo, Inc.). Since joining NTT, he has been engaged in the research of modulation/demodulation techniques for mobile radio, and research and development of wireless access technologies for WCDMA mobile radio and broadband wireless packet access technologies beyond IMT-2000. He is

now director of the Wireless Access Laboratory of NTT DoCoMo. He is a member of the Institute of Electronics, Information, and Communication Engineers (IEICE) of Japan.

KENICHI HIGUCHI received his B.S. degrees from Waseda University, Tokyo, Japan, in 1994. In 1994, he joined NTT Mobile Communications Network, Inc. (now, NTT DoCoMo, Inc.). Since then he has been engaged in the research and development of code synchronization and interference canceller technique for wideband DS-SS-CDMA mobile radio systems. He is a member of the IEICE of Japan.

SHINYA TANAKA received his B.S. degree from Waseda University, Tokyo, Japan in 1993. In 1993 he joined NTT Mobile Communication Network, Inc. (NTT DoCoMo). Since joining NTT DoCoMo, he has been engaged in the research and development of adaptive antenna arrays for DS-SS-CDMA. He is a member of the IEICE of Japan.

FUMIYUKI ADACHI [M'79-SM'90] received his B.S. and Dr. Eng. degrees in electrical engineering from Tohoku University, Sendai, Japan, in 1973 and 1984, respectively. In April 1973 he joined the Electrical Communications Laboratories of Nippon Telegraph & Telephone Corporation (now NTT) and conducted various types of research related to digital cellular mobile communications. From July 1992 to December 1999, he was with NTT Mobile Communications Network, Inc. (now NTT DoCoMo, Inc.), where he led a research group on wideband/broadband CDMA wireless access for IMT-2000 and beyond. Since January 2000 he has been at Tohoku University, Sendai, Japan, where he is a professor of electrical and communication engineering at the Graduate School of Engineering. His research interests are in CDMA and TDMA wireless access techniques, CDMA spreading code design, Rake receivers, transmit/receive antenna diversity, adaptive antenna array, bandwidth-efficient digital modulation, and channel coding, with particular application to broadband wireless communications systems. From October 1984 to September 1985 he was a United Kingdom SERC Visiting Research Fellow in the Department of Electrical Engineering and Electronics at Liverpool University. From April 1997 to March 2000 he was a visiting professor at Nara Institute of Science and Technology, Japan. He has published over 160 papers in journals and over 70 papers in international conferences. He is a member of IEICE and was a co-recipient of the IEICE Transactions Best Paper of the Year Award in 1996 and 1998.

The Swiss Federal Institute of Technology Zurich (ETHZ)

invites applications for a

Professor/Assistant Professor (with Tenure Track) of Mobile Computing Systems

The primary aim of this position is to strengthen research and teaching in modern mobile communication and information systems. The candidate is expected to promote research on the system level, in areas such as ubiquitous computing, wearable computing, mobile embedded systems.

Candidates should have established an internationally recognized track record in their area. We are seeking individuals willing to cooperate with other faculty and with research partners. The rank (full/associate/assistant professor with tenure track) will depend on the candidate's qualifications.

Applications for this position should contain a curriculum vitae, a list of publications, a list of research activities and a research statement, and should be submitted to the President of ETH Zürich, Prof. Dr. O. Kübler, ETH Zentrum, CH-8092 Zürich, no later than February 15, 2001. The ETHZ specifically encourages female candidates to apply with a view towards increasing the proportion of female professors.

Questions referring to this position should be mailed to Prof. Dr. B. Plattner, ETH Zentrum, CH-8092 Zurich (E-mail: plattner@tik.ee.ethz.ch).